LOW EMITTANCE INJECTOR AT SCSS

Hitoshi Tanaka*[A,B)], Kazuaki Togawa[A)], Hitoshi Baba[A)], Toru Hara[A,B)], Atsushi Higashiya[A)], Takahiro Inagaki[A)], Hirokazu Maesaka[A)], Hiroshi Matsumoto[B,C)], Kazuyuki Onoe[A)], Yuji Otake[A)], Katsutoshi Shirasawa[A)], Takashi Tanaka[A,B)], Takanori Tanikawa[A)], Makina Yabashi[A,B)], Tsumoru Shintake[A)],

A) RIKEN/SPring-8, 1-1-1, Kouto, Sayo, Hyogo, 679-5148, Japan
B) JASRI/SPring-8, 1-1-1, Kouto, Sayo, Hyogo, 679-5198, Japan
C) KEK, 1-1, Oho, Tsukuba, Ibaraki, 305-0801, Japan.

Abstract

The SPring-8 compact SASE source (SCSS) project aims at SASE-based FEL at wavelength region of 1 angstrom. To generate a high quality electron beam, a low emittance injector comprising of a 500 kV pulsed electron gun, beam deflector and three-stage velocity bunching process has been investigated [1, 2]. To confirm beam performance of the injector, the SCSS prototype accelerator with the identical injector system was constructed [3]. Via beam tuning of the prototype accelerator over half a year, the first stage beam commissioning was completed successfully and SASE at wavelength of about 50 nm was observed in June 20th, 2006 [3]. The analysis of experimental SASE data predicts that essential beam quality, i.e., "effective electron beam brilliance" reaches to the target value, 200 $A/\pi^2 mm^2 \cdot mrad^2$. In this paper, we describe the injector design of the SCSS prototype accelerator and show the achieved beam performance.

INTRODUCTION

In order to achieve SASE-based x-ray FEL, normalized slice emittance of ~1 πmm.mrad is required with a high peak current of a few kA. For this purpose, it has been believed that a photo-cathode RF electron gun (RF-gun) based system is the most promising. The RF-gun based system has been thus adopted as the injector for the LCLS [4] and XFEL [5] projects.

In the SCSS project, we however took a different approach to this problem. A conventional technology-based injector, which comprises of a pulsed electron gun with a thermionic-cathode, a beam deflector and three-stage velocity bunching process was chosen [1, 2]. This choice is due to potentiality achieving simultaneously high stability and tunability, which are critically important for realization of "stable" x-ray FEL. This injector system is free from the dark current from the cathode, which could be a serious problem in the RF-gun based system.

In the SCSS injector system, basic functions on beam handling such as emission of electrons, beam pulse processing, beam acceleration and bunch compression are separated. Machine parameters in each function are thus adjustable independently, which assures wide tunability in operation. This is an advantage when compared to the RF-gun based system, where these functions are tightly coupled. Furthermore, the RF-gun based system has to use a state of the art laser system to extract electrons from the cathode, which may cause instability in the initial beam condition.

Although the SCSS injector system has an advantage on the electron beam stability and operation tunability, there remains the question whether "emittance conservation" through the injector is a sufficient level or not under the practical error condition. To reply this, in other words, to confirm beam performance of the injector and investigate hidden problems in operation, the SCSS prototype accelerator was constructed and has been tested.

OUTLINE OF INJECTOR SYETEM

Figure 1 shows the schematic view of the injector system of the SCSS prototype accelerator. Since the SCSS injector is basically the same as that of the prototype accelerator, we explain beam handling over the injector by using Fig. 1.

Electron beams are extracted from the single crystal CeB_6 cathode by a 500 kV pulse voltage (1 in Fig. 1) [6]. The repetition rate is 60 Hz at most and the electron pulse width is about 2 μsec. The theoretical thermal emittance is 0.4 πmm.mrad. The initial beam energy is 500 keV and peak current is 1 A.

The developed beam deflector (2 in Fig. 1) cuts out about 1 nsec short pulse from the extracted beam. Due to the fast rising and falling time of the deflector electric field, 1 nsec beam pulse has a beam tail of about 100 psec, in front of and behind the beam. The deflector has a collimator with a hole of which diameter is 5 mm and the beam is collimated into a cylindrical shape with a transversally hard edge.

Owing to the high beam energy of 500 keV, a conventional solenoid coil, which covers a wide beam path, is unnecessary. Instead of the solenoid, a special magnetic lens, where the solenoid coil is covered by an iron york, has been developed (3 in Fig. 1). This magnetic lens has two significant advantages: (1) Due to the localized focusing field, three functions, beam focusing, beam acceleration and bunch compression can be separated. (2) Due to the properly large aperture, nonlinear fringe fields are suppressed enough to avoid the

* E-mail: tanaka@spring8.or.jp

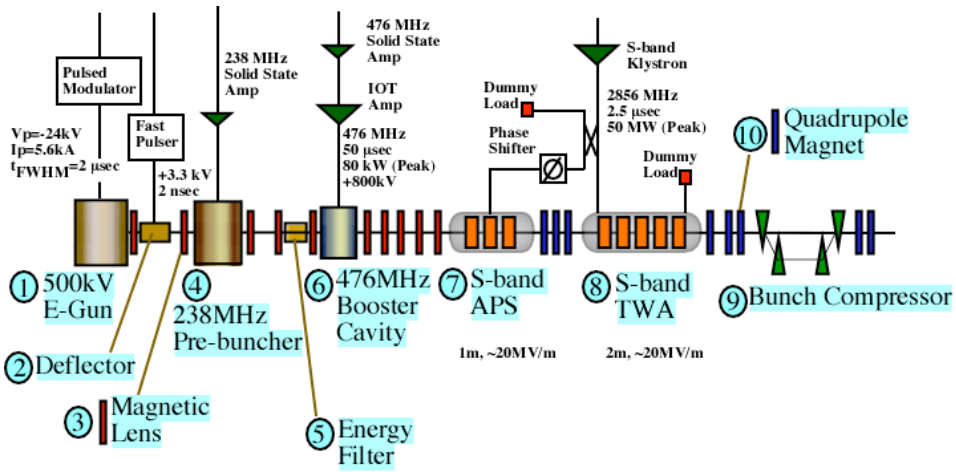

Fig. 1: Schematic drawing of SCSS injector system.

emittance growth. The former advantage is quite important for precise beam tuning.

The cylindrical beam with the pulse width of 1 nsec receives energy modulation, about 400 keV in a peak-to-peak value, in the 238 MHz pre-buncher (4 in Fig. 1). The energy modulated beam develops the density modulation when passing through a 1.6 m drift section. The energy filter (5 in Fig. 1) is now not used. In front of the booster, the average beam energy is ~0.43 MeV and the peak current reaches to 5 A (~200 ps). Then, in the 476 MHz booster cavity (6 in Fig. 1), the beam energy is boosted up to ~1 MeV to suppress the space charge effect and to linearlize the velocity gradient. In the velocity bunching process, both the voltage and phase of the two cavities are crucial for the bunching performance. Structures of both cavities were therefore carefully designed so that the frequency and gap-voltage are not sensitive against a vibration and temperature change. The peak current increases up to 50 A (~10 ps) while the 1 MeV electron beam flights over 1.3 m from the booster to the first S-band acceleration tube (7 in Fig. 1).

The energy of the electron beam is boosted by the two S-band accelerating tubes (7 and 8 in Fig. 1) up to ~41 MeV with the design bunching phase and up to~50 MeV with the crest phase. To suppress the emittance growth due to the symmetry-break of the first acceleration tube, APS structure was adopted. The velocity bunching process completes by the end of the first tube, where the peak current reaches to ~80 A (~6 ps).

Downstream of the first S-band accelerator tube, the beam energy is higher than 10 MeV and a quadrupole magnet (10 in Fig. 1) is used to focus the beam instead of the magnetic lens.

In the SCSS prototype accelerator, the beam is further compressed for SASE experiments by the bunch compressor, which comprises of four identical rectangular magnets (10 in Fig. 1). The deflecting angle is 0.1 rad and the maximum linear dispersion is about 110 mm. After the bunch compression, the peak current reaches to ~800 A (~0.7 ps).

The injector system is divided into three main parts, the electron gun, the beam deflector and three-stage velocity bunching process. Details of each part are described in the following three sections.

500 KV PULSED ELECTRON GUN

To constantly obtain low emittance electron beam with high beam current of 1~3 A, the electron gun was significantly improved from conventional electron guns. Table 1 lists the main electron gun parameters and Fig. 2 shows the CeB_6 cathode assembly (left) and the cathode being heated in the test chamber. The major improvements are:

- A small sized single crystal CeB_6, of which diameter is 3mm, was used as a cathode.
- The control grid was removed from the cathode, because the grid increases beam emittance by distorting the electric field.
- The gun voltage was raised up to 500 kV to suppress a space charge effect and remove troublesome solenoid coils.
- The cathode was stably heated up to high temperature as 1400~1600 deg.C by use of graphite heater.

Table 1: Gun Parameters

Beam Energy	500 keV
Peak Current	1~3A
Pulse Width (FWHM)	2 μsec
Repetition Rate	60 Hz
Cathode Temperature	1400~1600 deg.C
Cathode Diameter	3mm
Theoretical Thermal Emittance (rms)	0.4 πmm.mrad
Measured Normalized Emittance (rms, 90% particles)	0.6 πmm.mrad [7]

- The graphite sleeve surrounding the cathode was adopted to reduce beam halo.
- The flat Wehnelt was used as the anode to reduce emittance growth and to enlarge dynamic range of the peak current.

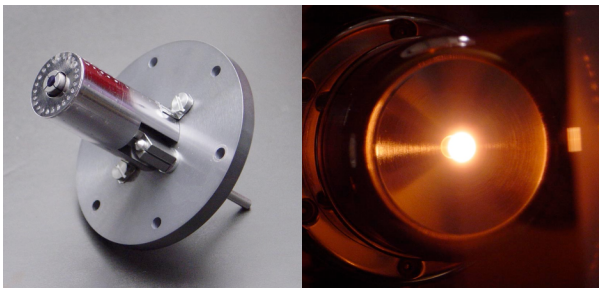

Fig. 2: Cathode assembly (left) and heated cathode (right).

BEAM DEFLECTOR

Since the control grid was removed from the developed electron gun to suppress beam emittance growth, beam deflector, which cuts out a 1nsec short pulse from the long one, is indispensable for the SCSS injector system. Figure 3 shows the principle of the beam deflector. The deflector comprises of two parallel electrode plates and one steering coil. The coil generates a DC magnetic field in the horizontal plane, which deflects the beam vertically and dumps it by using the narrow physical aperture as shown in the figure. The short pulsed electric field in the vertical plane, which cancels out the vertical kick by the DC magnetic field, achieves gating of ~1 nsec. The driving pulse has a fast rising and falling time, ~200 psec, which can generate a well-edged electron beam with a short tail. The flatness of the pulsed electric fields at the flat top determines the emittance degradation in the deflector. Hence, to achieve the sufficient field quality, impedance matching was fully considered in the design of the electric circuit and the parallel electrode plates including the casing chamber.

THREE-STAGE VELOCITY BUNCHING

The SCSS injector starts beam compression from the low beam energy of a 500 keV and reduces the bunch

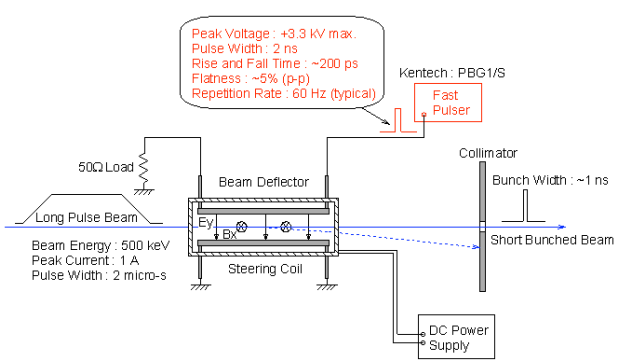

Fig. 3: Schematic drawing of beam deflector.

length by a several hundredth as the energy increases up to a few tens MeV. In the design of the SCSS injector, it is thus important to suppress emittance growth caused by a space charge force. On the other hand, the high compression ratio, higher than hundred, is required. Hence, handling of nonlinearity in the compression process is important.

Suppression of Emittance Growth

Assuming that the beam transverse shape is round and hard-edged and all electro-magnetic potentials are axial-symmetric, equation of motion under a space charge force is described in a cylindrical coordinate by [8]

$$r'' + \frac{\gamma'}{\beta^2\gamma} r' + \frac{\gamma''}{2\beta^2\gamma} r + \left(\frac{qB}{2m_0 c\beta\gamma}\right)^2 r - \left(\frac{p_\theta}{m_0 c\beta\gamma}\right)^2 \frac{1}{r^3} - \frac{2I}{(\beta\gamma)^3 I_A} \frac{r}{r_m^2} = 0, \quad (1)$$

where r, β, γ, B, p_θ, I, I_A and r_m are the electron radius, relative velocity, relative energy, longitudinal magnetic field, azimuthal momentum, peak current and Alfven current, respectively. The last term in L.H.S. shows the space charge force acting on the electron beam, suggesting that the guideline on the bunch compression is the ratio of γ^3. For example, when γ increases from 1 to 2, criterion on the compression ratio is $(2/1)^3=8$. This idea was first proposed by T. Shintake [1].

The bunch compression in the SCSS prototype accelerator however, apparently exceeds the above guideline and the simulation code, PARMELA predicts that the emittance growth is larger than that in 8-GeV SCSS. Because the injector parameters of the prototype accelerator were optimized not for SASE in wavelength region of 1 angstrom, but for in VUV region under the limited boundary condition, the peak current rather than the slice emittance was pursued. In the 8-GeV SCSS design, RF parameters, especially the RF voltage of 238 MHz pre-buncher will be re-optimized and the use of L-band accelerators instead of the S-band (7 and 8 in Fig. 1) is under investigation.

Nonlinearity Handling

To achieve the high compression ratio, suppression of nonlinearity in the bunch compression process, which originates from a RF voltage and velocity dependence on relative energy of the beam, is the key. For the simple system comprising of a RF potential, drift space and initially mono-energetic beam, the condition achieving the linear velocity distribution against time can be easily solved by neglecting a space charge force and expressed using only three parameters: an initial beam energy, peak RF voltage and RF phase. By using 500 keV and 209 kV as the initial beam energy and peak RF voltage of the pre-buncher, respectively, the linear distribution is obtained at about -125 deg. from the crest phase. Since the injector of the prototype accelerator has the 476 MHz booster cavity downstream of the pre-buncher, the condition for the

linear distribution becomes more complicated at the exit of the booster, i.e., it also depends on the booster parameters. Figure 4 shows the velocity distribution dependence on RF phase of the pre-buncher behind the booster, which was calculated with the injector parameters of the prototype accelerator. In this case the phase between -100 and -120 deg. is found to be optimum. In consideration of the experimental results obtained at the prototype accelerator, all the parameters relating to the three-stage velocity bunching process have been re-investigated.

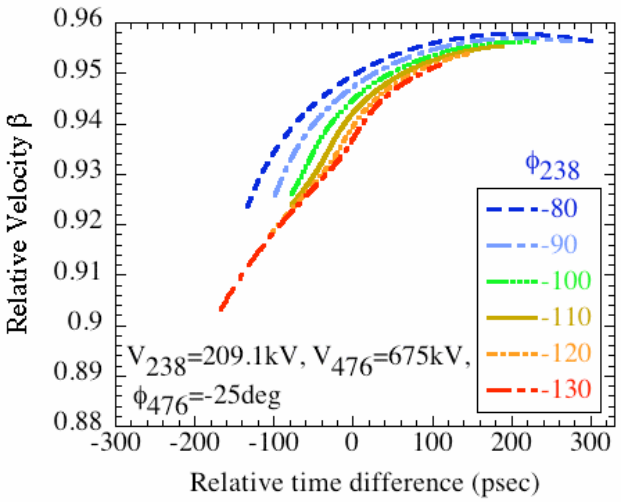

Fig. 4: Velocity distribution dependence on RF phase of the pre-buncher behind the booster calculated with the injector parameters of the prototype accelerator.

SCSS PROTOTYPE ACCELERATOR

The SCSS prototype accelerator comprises of the low emittance injector, bunch compressor with a magnetic chicane, C-band acceleration system, and two in-vacuum undulators as shown in Fig. 5. To verify the injector capability providing the high quality electron beam, the design target of the normalized slice emittance and peak current was set at 2 πmm.mrad and 800 A, respectively. Attainment of the target confirms that the beam performance for x-ray FEL is reachable by smooth extension of the prototype accelerator. And also, the target performance is enough for SASE lasing at wavelength of 40 ~ 60 nm.

Since both the injector and bunch compressor were already described in the previous sections (see Fig. 1), we start a brief explanation of the prototype accelerator from the C-band acceleration system. The system is divided into two acceleration units. Each unit has two 1.8 m-long choke-mode type traveling wave acceleration (TWA) tubes [9] driven by a 3/4π mode. Each unit has one 50MW C-band klystron. The RF power from the klystron is boosted up by a factor of 3.4 by the RF pulse compressor and equally fed to the two acceleration tubes. In the prototype accelerator, different compressors, SKIP [10] and SLED [11] were adopted for the first and second units, respectively, to compare the performance of the two compressors. The nominal accelerating field gradient is about 30 MV/m when the beam is accelerated at the crest phase and in this operating condition RF power fed to each acceleration tube is 46 MW on average of 300 nsec filling time.

The undulator part is divided into two identical in-vacuum undulators of 4.5 m. The permanent magnet material is NdFeB and magnet structure is a 45-deg. tilted Halbach type [12]. Minimum, nominal and fully opened gaps are 2, 3 and 25 mm, respectively. At the minimum (nominal) gap K-value reaches to about 1.8 (1.3) and the wavelength of the first harmonic is about 80 (60) nm with the beam energy of 250 MeV. The period length is 15 mm and the number of periods is 300 per undulator. To keep a small beam size in the horizontal plane, one focusing quadrupole locates between two undulators. In front of the first undulator, a magnet chicane is installed to protect the undulator permanent magnets from accidental electron bombardments and dark currents from the C-band accelerators.

The symbol “M” in Fig. 5 shows a chamber port for a usual beam profile measurement with fluorescence and optical transition radiation. In the beam tuning, these ports are also used to measure a longitudinal beam density distribution by using coherent transition radiation because evolution of the longitudinal distribution is quite important for setting RF parameters in the velocity bunching process. The symbol “S” shows a transverse beam slit to collimate the beam in energy and transverse space.

TUNING STRATEGY OF SCSS PROTOTYPE ACCELERATOR

In the beam tuning, the following points were well considered, because there is no diagnostics to measure the slice emittance directly.

(1) Suppression of slice emittance growth by a space charge force: Over-focusing of the beam causes the emittance growth by a space charge force and hence, it is important to tune the real beam envelope same as the calculation. To this end, initial condition of the real beam from the electron gun should be fixed. We made series of systematic measurements on the beam profiles by changing strengths of the plural magnetic lenses one by one without RF power of both the 238 MHz pre-buncher and 476 MHz booster. By analyzing the data, the virtual beam source was thus determined for the prototype accelerator.

(2) Suppression of slice emittance growth by over-bunching: RF voltage and phase were calibrated and set based on the real beam response for the pre-buncher, booster and S-band accelerators. As the beam response, dependences of the bunch compression on these two parameters were measured. The measurements were performed with the developed microwave spectrometer and the detection system combining the wide frequency band diode detector [13] with a high-pass mesh filter. For

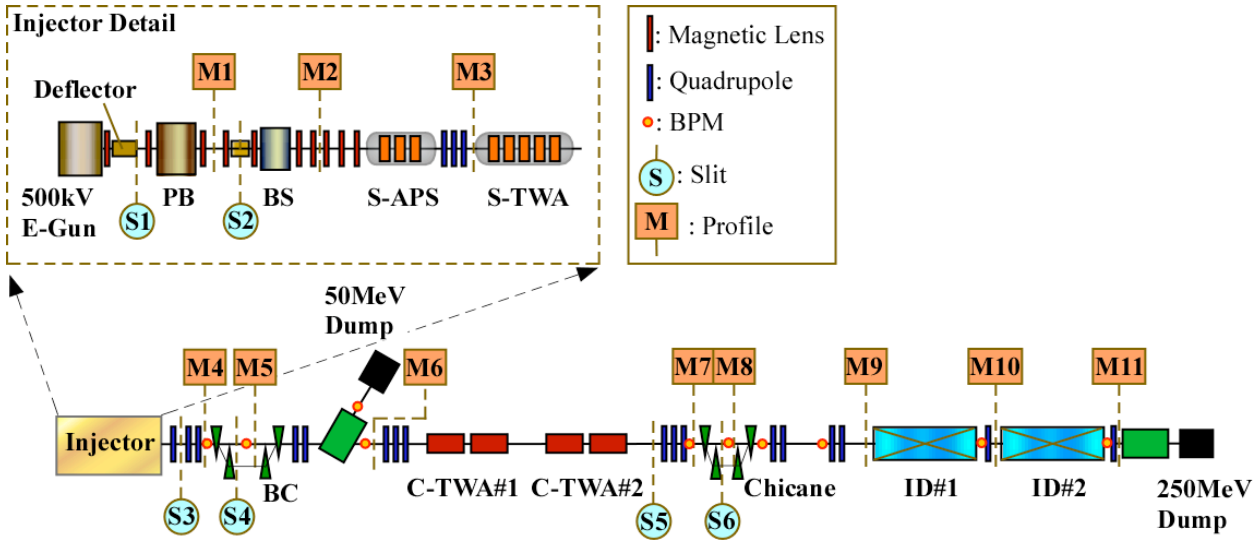

Fig. 5: Schematic drawing of SCSS prototype accelerator.

the crest phase detection, we used the following three methods depending on the condition; beam induced field method [14], the method based on the maximum beam transmission and the method based on the maximum displacement at the dispersive section.

(3) Suppression of slice emittance growth by nonlinear fields: Nonlinear fields at both fringes of the magnetic lenses and RF cavities increase the slice emittance. To suppress this growth, electron beam centering to each device is important. We centered the beam on each device by dithering, i.e., by observing the beam responses against the current and acceleration phase modulation.

(4) Confirmation of slice emittance: Condition of the transverse phase space was indirectly confirmed by comparing the measured data with the simulated ones. For the comparison, five beam profiles upstream of the C-band acceleration system and three kinds of projected emittance were used.

EXPERIMENTAL RESULTS OBTAINED AT SCSS PROTOTYPE ACCELERATOR

In this section, we summarize the obtained results, i.e., the projected emittance, bunch length, dark current, stability and electron beam brilliance.

Projected emittance

The projected emittance values were measured under the following three conditions: (1) 500 keV beam with the pulse-width of 1nsec after the beam deflector (M2 in Fig. 5), (2) 50 MeV beam accelerated at the crest phase of the S-band TWA tube (M6 in Fig. 5), and (3) 250 MeV beam accelerated at the bunching phase (crest -30 deg.) of the S-band TWA tube and at the crest phase of the C-band TWA tubes (M9 in Fig. 5). The emittance of condition (1) was estimated from the beam size and angular divergence measured by the horizontal slit scan. On the other hand, the emittance of the conditions (2) and (3) were estimated by a conventional Q-scan method. Table 2 lists the estimated emittance values together with the calculated ones. The measured emittance of the long pulse beam emitted from the electron gun is also shown. Comparing the emittance values with and without the deflector, we see that the emittance growth by the deflector is not significant. We also see that the estimated values have good agreement with the calculation at the beam energy of 50 and 250 MeV.

Fig. 6 shows the beam size dependences obtained by the Q-scan method at the beam energy of 50 MeV. Each point represents the average of 10 data. The solid and dashed lines represent the fitting curves of which form is determined by linear beam theory. Since scattering of 10 data is smaller than the radius of the plotted circles, it was neglected in the figure. The error bar represents 1σ of a fitting error. We see that the all data points over the wide range of the focusing strength are well fitted by the parabolic curve. These facts show that the electron beam is stable enough for this kind of measurement.

Bunch length

Bunch length was measured with a femto-second streak camera (Hamamatsu Photonics FESCA-200, temporal resolution of 200 fs). Cherenkov radiation from conically shaped BK7 glass was observed for the 41MeV electron beam and optical transition radiation (OTR) from an Au

Table 2: Estimation of normalized emittance

Beam Energy [MeV]	Norm.Emittance (ε_x, ε_y) [πmm.mrad]	Calculation (ε_x, ε_y) [πmm.mrad]
0.5(bef.deflector)	(0.6, -)	-
0.5(aft.deflector)	(1, -)	-
50	(3, 3)	(2.8, 2.6)
250	(4, 2)	(2.3, 2.3)

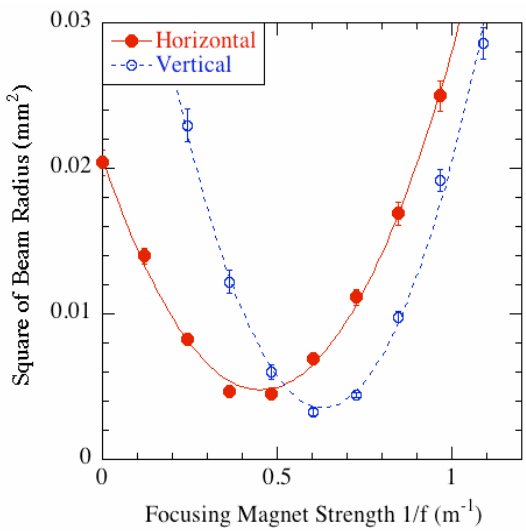

Fig. 6: Measured data by the Q-scan method at the beam energy of 50 MeV.

thin film was observed for the 250 MeV electron beam. The results are 5 psec (41 MeV) and 2 psec (250 MeV) in 1σ, which are much larger than the simulated bunch length of 1 psec. As causes of this discrepancy, we presently predict that the transverse beam size enlarges the pulse length of Cherenkov radiation. And also, in respect to measurement with OTR, we doubt that the optics including streak camera system enlarges the pulse length.

We measured bunch length with another method, where the pulse length of beam is converted to a systematic energy chirp by using a RF field gradient [15]. In our case, the second C-band acceleration unit (C-TWA#2 in Fig. 5) is operated at a zero-crossing phase to generate a systematic energy chirp. Beam density distribution projected to the horizontal plane is then observed with OTR from the Au thin film located in the middle of the chicane (M8 in Fig. 5). The linear dispersion at the OTR screen is about 150 mm. Figure 7 shows the measured density profiles under three different operating conditions of the second C-band unit, i.e., RF turned off and at the crest ± 90 deg. accelerating phase. By using the RF parameters and dispersion value, the full pulse width is estimated to be about 1.1 ps, which agrees well with the simulation.

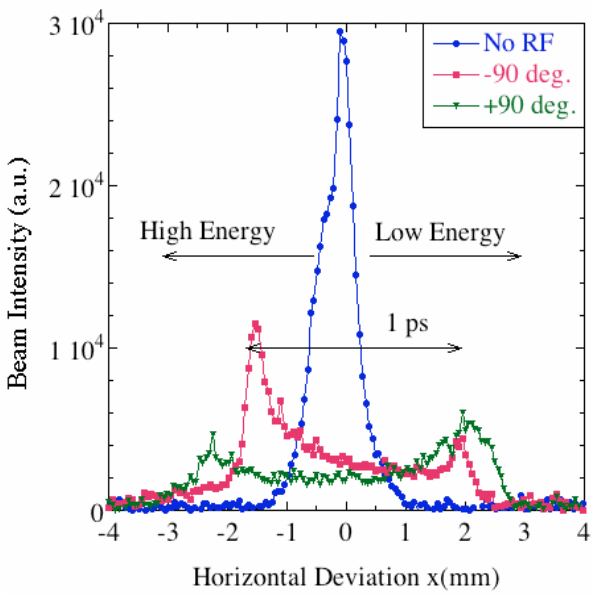

Fig. 7: Measured beam density profile projected on the horizontal plane with three different operating conditions.

Dark current

When the deflector is switched on, dark current downstream of the pre-buncher is invisible on a fluorescence screen of M1 in Fig. 5. It is true that the dark current from the electron gun is negligible for any beam tuning. Quantitative measurements are planned in next operation period after the summer shutdown.

Stability

Long-term stability of the electron beam or the prototype accelerator is the following. The standard SASE lasing is basically reproduced by reloading the nominal parameter set of the magnets and RF systems. At present, the SCSS prototype accelerator has not been operated continuously over a long period, but operated day by day. In 2 to 3 hr after the operation starts in the morning, we suffer the slow drifts of some parameters such as the high voltage of the electron gun, etc, which is so far adjusted manually. Introduction of slow feedback controls is thus under investigation.

With respect to short-term stability of the electron beam, the stability of the beam energy is 0.37 % in full-width downstream of the second C-band acceleration unit. This was estimated by using the shot-by-shot fluctuation of the horizontal position at M8 in Fig. 5. The beam orbit stability was measured by using the beam position monitor (BPM) [16] at the entrance of the first undulator, where no linear dispersion exists in the design. The horizontal and vertical orbit stabilities at this position are 13 and 21 μm in 1σ, respectively. These values are smaller than a fifth of the beam size.

With respect to lasing stability, the peak performance has not been achieved routinely. In order to maximize the laser amplification, slight tuning is needed for the pre-buncher phase, S-band TWA phase, position and width of the slits, S4 and S6 in Fig. 5. Figure 8 shows the shot-by-shot lasing stability measured by the photodiode (International Radiation Detectors Inc. SXUV100) in the VUV beamline [17]. The energy per pulse was measured by integrating the photogenerated charge of the photodiode. The lasing wavelength is about 60 nm and the repetition rate was 5 Hz. The data however were taken asynchronously at 3 Hz due to the reading speed of the temporary data acquisition system. We see that relatively strong lasing occurred in all shots over the period of measurement without any feedback correction.

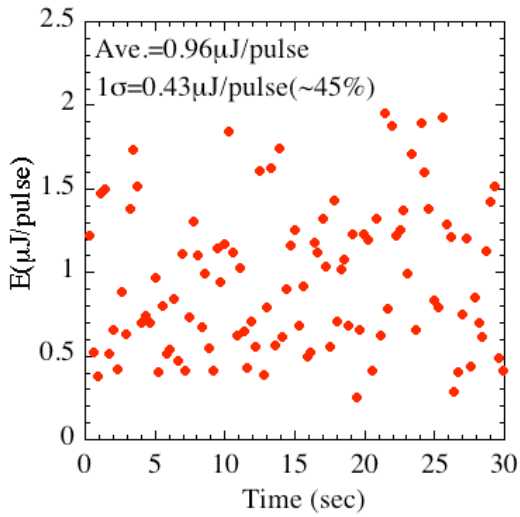

Fig. 8: Shot-by-shot stability of lasing. The beam energy is 250 MeV and the undulator gap is 3 mm.

Electron beam brilliance

Effective electron beam brilliance, the ratio of a peak current to 4-dimensional transverse phase space volume, is estimated by the following two approaches. One is to reproduce the measured dependence of the laser amplification on the peak current by using the 1-D model [18]. The other is to reproduce the measured dependence of the laser amplification on the K-value by using the 3-D simulation code, SIMPLEX [19].

(1) Estimation with 1-D model: The bunch current was controlled with the slit S4 in Fig. 5. Through the bunch length measurement with a systematic energy chirp, we confirmed that the local density peak in the bunch depends on the slit width of S4. Figure 9 shows the dependence measured by the photodiode in the VUV beamline. The filled circles and error bars represent the average and 1σ of 100 data, respectively. In this measurement, the gaps of both undulators were closed to 4 mm and the beam energy was accelerated up to the nominal energy, 250 MeV. Hence, the lasing wavelength is 49nm.

In the 1-D model, the total radiation intensity I is written by the sum of the spontaneous radiation intensity I_N and coherent radiation intensity I_L as

$$I = I_L + I_N = I_{L0}\exp\left(z/L_{1G}\right) + I_N, \qquad (2)$$

where z and L_{1G} represent the total length of the undulators and the 1-D gain length, respectively. Assuming that the horizontal normalized slice emittance is the same as the vertical one, L_{1G} is expressed by using the beam parameters as

$$L_{1G} = \frac{150.2}{\left(\dfrac{H}{\left\langle\beta_x^{1/2}\right\rangle\left\langle\beta_y^{1/2}\right\rangle}\right)^{1/3}}, \quad H = \frac{I_p}{\varepsilon_{ns}}. \qquad (3)$$

Here, ε_{ns} and I_p represent the normalized slice emittance and peak current, respectively. β_x and β_y are the horizontal and vertical betatron functions, respectively. The bracket < > represents the average of the inside parameter over the undulator length. First we determined the betatron functions experimentally. Then, we fitted the experimental data by using H as only a parameter in consideration with the dependence of Eq. (2) and (3) on the beam charge. The solid line in Fig. 9 shows the result, which agrees well with the experimental data. The ratio of I_p to ε_{ns}, namely H is estimated to be 480 A/πmm·mrad. Assuming that ε_{ns} is the design value, 2 πmm·mrad, the electron beam brilliance becomes 240 A/π^{2}mm^2·mrad^2.

(2) Estimation with 3-D model: Fixing the electron beam condition, we measured the dependence of the angular photon flux density on the K-value by changing the gap of the first undulator only. To extract the core photon beam, the horizontal acceptance was limited within ±100μm from the beam center by using the horizontal slit in the VUV beamline. Then, the horizontally narrow beam was monochromatized and detected by the CCD camera [17]. We further set a small window on the CCD image for limiting the bandwidth and the vertical acceptance. The angular photon flux density was finally obtained by integrating the intensities in the window. Figure 10 shows the measured dependence of the angular flux density on the K-value with the filled circles. Each data was taken by the integration time of 10sec, i.e., the integration of 50 data. The vertical axis represents the ratio of the flux density to that of the spontaneous radiation. The spontaneous radiation data were measured for each K-value by operating S-band TWA at the de-bunching phase.

Assuming that the normalized slice emittance and momentum spread are the design values, 2 πmm.mrad and 0.1 % (1σ), respectively, we simulated the

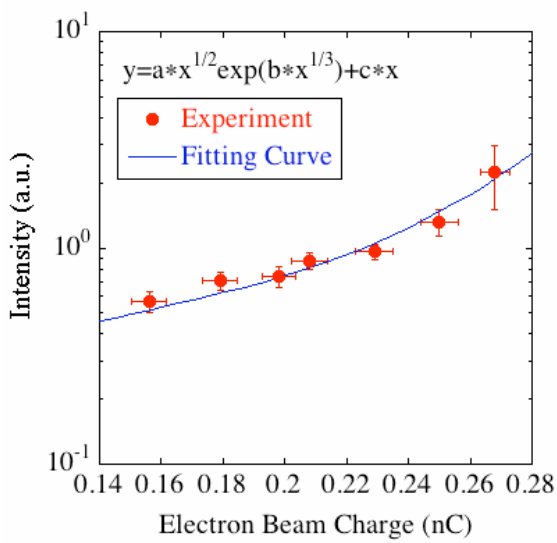

Fig. 9: Dependence of laser amplification on the beam charge.

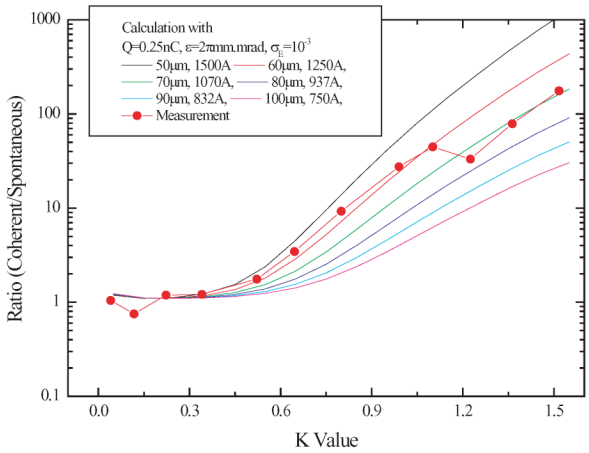

Fig. 10: Dependence of laser amplification on the K-value.

dependence on the K-value with SIMPLEX. Here, the peak current was used as a parameter. The solid lines in Fig. 10 show the results. By comparing the simulation and experimental data, we see that the experimental data locate between the two lines obtained with 1070A and 1250A. The electron beam brilliance is estimated to be 270 ~ 310 $A/\pi^2 mm^2 \cdot mrad^2$.

SUMMARY

The SCSS injector system was designed to achieve the stable and flexible beam operation satisfying the high beam quality required for SASE-based x-ray FEL. On the other hand, our design needs the bunch compression of relatively long electron beam in a low energy regime ranging from 500 keV to a few MeV, with suppressing the emittance growth due to a space charge force and non-linearity. This is quite challenging and there remains the question whether "emittance conservation" through the injector is a sufficient level or not under the practical error condition. To confirm beam performance of the injector, the SCSS prototype accelerator was constructed.

Owing to careful beam tuning based on the emittance conservation, SASE lasing in the wavelength ranging from 40 to 60nm has been stably obtained at the SCSS prototype accelerator. We analysed the reproducible SASE lasing data by the 1-D model and 3-D simulator. As a result, we found that electron beam brilliance is estimated to satisfy the design target, $200A/\pi^2 mm^2 \cdot mrad^2$.

This experimental result shows that PARMELA gives a good design guideline in our case and concludes that the beam performance for x-ray FEL is reachable by the smooth extension of the prototype accelerator.

REFERENCES

[1] T. Shintake et al., "SPring-8 Compact SASE Source (SCSS)", SPIE, Optics for Fourth-Generation X-Ray Sources, Bellingham, August 2001, p. 12.

[2] "SCSS X-FEL Conceptual Design Report", RIKEN/SPring-8, May 2005, Mikazuki, Japan, http://wwwxfel.spring8.or.jp/.

[3] T. Shintake, "Status of the SCSS Test Accelerator and XFEL Project in Japan", EPAC'06, Edinburgh, June 2006, p. 2741; http://www-xfel.spring8.or.jp/fist_lasing/FirstLasingofSCSS.html.

[4] "Linac Coherent Light Source (LCLS) Conceptual Design Report", SLAC-R-593, April 2002.

[5] "TESLA Technical Design Report, PART V, The X-ray Free Electron Laser", ed. G. Materlik and Th. Tschentscher, March 2001.

[6] K. Togawa et al., "CeB6 Electron Gun for the Soft X-ray FEL Project at SPring-8", NIMA, **528** (2004) 312.

[7] K. Togawa et al., "Emittance Measurement on the CeB_6 Electron Gun for the SPring-8 Compact SASE Source", FEL'04, Trieste, August 2004, p.351.

[8] M. Reiser, "Theory and Design of Charged Particle Beams", John Wiley & Sons, Inc., New York, 1994, p. 210.

[9] T. Shintake et al., "HOM-Free Linear Accelerating Structure for e+e- Linear Collider at C-band", PAC'95, Dallas, May 1995, p. 649.

[10] T. Sugimura et. al, "SKIP–A Pulse Compressor for SuperKEKB", LINAC'04, Lübeck, August 2004, p.754 (2004).

[11] T. Shintake et al., "A New RF Pulse-Compressor Using Multi-Cell Coupled-Cavity System", EPAC'96, Sitges, June 1996, p. 2146.

[12] T. Tanaka et al., "Development of the short-period undulator for the X-ray FEL project at SPring-8", SRI'03, San Francisco, August 2003, p. 227.

[13] International Radiation Detector Inc., http://www.ird-inc.com/.

[14] R. B. Neal, "The Stanford Two-Mile Accelerator-I", W. A. Benjamin, Inc., New York, 1968, p.383.

[15] L. Rivkin et al., "Bunch Lengthening in the SLC Damping Ring", EPAC'88, Rome, June 1988, p.634.

[16] T. Shintake, "Development of Nanometer Resolution RF-BPMs", HEACC'98, Dubna, October 1998, http://lcdev.kek.jp/Conf/HEACC98/133.PDF .

[17] M. Yabashi et al., in these proceedings.

[18] R. Bonifacio et al., "Collective Instabilities and High-Gain Regime in a Free Electron Laser", Opt. Commun., **50** (1984) 373.

[19] SIMPLEX was developed by Takashi Tanaka (RIKEN/SPring-8), http://radiant.harima.riken.jp/simplex/.